The Astrophysical Journal, 692:1321–1332, 2009 February 20 doi:10.1088/0004-637X/692/2/1321

CONSTRAINING THE NFW POTENTIAL WITH OBSERVATIONS AND MODELING OF LOW SURFACE BRIGHTNESS GALAXY VELOCITY FIELDS

Rachel Kuzio de Naray[1,4], Stacy S. McGaugh[2], and J. Christopher Mihos[3]
[1] Center for Cosmology, Department of Physics and Astronomy, University of California, Irvine, CA 92697-4575, USA; kuzio@uci.edu
[2] Department of Astronomy, University of Maryland, College Park, MD 20742-2421, USA; ssm@astro.umd.edu
[3] Department of Astronomy, Case Western Reserve University, 10900 Euclid Avenue, Cleveland, OH 44106, USA; mihos@case.edu
Received 2008 July 1; accepted 2008 October 24; published 2009 February 24

ABSTRACT

We model the Navarro–Frenk–White (NFW) potential to determine if, and under what conditions, the NFW halo appears consistent with the observed velocity fields of low surface brightness (LSB) galaxies. We present mock DensePak Integral Field Unit (IFU) velocity fields and rotation curves of axisymmetric and nonaxisymmetric potentials that are well matched to the spatial resolution and velocity range of our sample galaxies. We find that the DensePak IFU can accurately reconstruct the velocity field produced by an axisymmetric NFW potential and that a tilted-ring fitting program can successfully recover the corresponding NFW rotation curve. We also find that nonaxisymmetric potentials with fixed axis ratios change only the normalization of the mock velocity fields and rotation curves and not their shape. The shape of the modeled NFW rotation curves does not reproduce the data: these potentials are unable to simultaneously bring the mock data at both small and large radii into agreement with observations. Indeed, to match the slow rise of LSB galaxy rotation curves, a specific viewing angle of the nonaxisymmetric potential is required. For each of the simulated LSB galaxies, the observer's line of sight must be along the minor axis of the potential, an arrangement that is inconsistent with a random distribution of halo orientations on the sky.

Key words: dark matter – galaxies: kinematics and dynamics

Online-only material: color figures

1. INTRODUCTION

Cosmologically motivated numerical simulations of cold dark matter (CDM) describe very specifically the properties of the dark matter halos that should be observed in the universe. The simulations show that CDM halos are cuspy, meaning that the density of the halo, regardless of its mass, rises very steeply toward the center (e.g., Dubinski 1994; Navarro et al. 1996, 1997; Moore et al. 1999; Reed et al. 2003; Diemand et al. 2005). The simulations also dictate the range of permissible values of halo parameters based on the assumed cosmology of the simulations. The concentration c of a halo, for example, depends on the density of the universe at the time the halo forms, which in turn depends on the adopted values of h, Ω_m, σ_8, etc. (Navarro et al. 1996, 1997). Due to this intimate connection to cosmology, the values of halo parameters are not arbitrary.

The most well known description of CDM halo behavior is the cuspy Navarro–Frenk–White (NFW) halo where $\rho \sim r^{-1}$ (Navarro et al. 1996, 1997). The rotation curves of these halos are parameterized by two numbers: the concentration, c, and a characteristic velocity, V_{200}. These two parameters cannot freely vary nor can they vary independent of the other; there is a correlation between c and V_{200} (e.g., Navarro et al. 1997; Jing 2000; Bullock et al. 2001; Wechsler et al. 2002). This c–V_{200} relation, combined with the cosmological constraints on c, means that the expected rotation curve for a CDM halo of a given mass is well determined.

Though the need for dark matter in disk galaxies has long been indicated by flat rotation curves (e.g., Rubin et al. 1980; Bosma 1981), it has been less obvious that the dark matter halos are consistent with cuspy CDM halos. Because low surface brightness (LSB) galaxies are thought to be dark matter-dominated down to small radii (de Blok & McGaugh 1996; de Blok & McGaugh 1997; Borriello & Salucci 2001, but see Fuchs 2003), their kinematics have been used as probes of the density distribution of galaxy mass dark matter halos. Rotation curves derived from H I velocity fields and long-slit Hα observations are frequently consistent with halos having a cored $\rho \sim r^0$ density distribution (e.g., Flores & Primack 1994; de Blok et al. 1996; de Blok & Bosma 2002; Marchesini et al. 2002; Côté et al. 2000) rather than the steeper profile of the NFW halo. This result has also been supported by rotation curves derived from high-resolution two-dimensional velocity fields obtained with integral field spectrographs (e.g., Chemin et al. 2004; Gentile et al. 2005; Simon et al. 2005; Kuzio de Naray et al. 2006, 2008).

In Kuzio de Naray et al. (2006, 2008, hereafter K06 and K08, respectively), we presented DensePak Integral Field Unit (IFU) Hα velocity fields, rotation curves, and halo fits for a sample of 17 LSB galaxies. We fit both a cored pseudoisothermal halo ($\rho \sim r^0$) and a cuspy NFW halo ($\rho \sim r^{-1}$) to the data and found the halo central densities and rotation curve shapes to be better described by the cored halo model. The NFW fits to the DensePak rotation curves were often found to have concentrations lower than what is expected for galaxies in a ΛCDM cosmology (see also Gentile et al. 2007, but see Swaters et al. 2003b for a different conclusion) and to favor a power spectrum having a lower amplitude on small scales (Zentner & Bullock 2002; McGaugh et al. 2003; K08). We found that the NFW rotation curves specified by the c–V_{200} relation (the rotation curves that our galaxies *should* have according to ΛCDM) are much more steeply rising than the observed DensePak rotation curves. In addition, these cosmologically consistent halos show a cusp mass excess at the centers of the galaxies, indicating that at least two times more mass

[4] NSF Astronomy and Astrophysics Postdoctoral Fellow.

is expected in the cuspy CDM halos than is allowed by the data.

CDM halos must be both cuspy and follow the c–V_{200} relation defined by ΛCDM. The density profiles of the K06 and K08 data are not well described by cuspy halos, nor do the galaxies fall on the c–V_{200} relation. These DensePak results are consistent with many previous long-slit and H I studies of LSB galaxies (e.g., de Blok et al. 2001; Bolatto et al. 2002; de Blok & Bosma 2002; Swaters et al. 2003a), as well as similar DensePak studies by Simon et al. (2005). Different observational techniques (with different data reduction and analysis procedures as well as sources of error) leading to similar conclusions suggests that perhaps the discrepancy between the NFW halo and the observations does not arise at the telescope or during data analysis, but is rather due to an incorrect assumption about the specific form of the NFW halo potential.

Our goal in this paper is to model the NFW halo to determine if, and under what conditions, it appears consistent with the observed data. Starting with an axisymmetric NFW potential, how must it be modified (e.g., introduction of an asymmetry) in order to appear consistent with both the observed two-dimensional velocity field and the derived rotation curve? We construct a model disk galaxy embedded in an NFW halo and then "observe" it in the same way as we have observed our sample of galaxies with DensePak. We then compare the mock velocity field and the derived mock rotation curve to the real galaxy data.

We adopt a numerical approach to investigating nonaxisymmetric halo potentials because once axisymmetry is broken, the data analysis becomes much more complicated. Noncircular motions and asymmetries are traditionally investigated by doing a higher-order Fourier decomposition of the velocity field (e.g., Schoenmakers et al. 1997; Wong et al. 2004). We have tried this approach, but it was not sufficiently well constrained for these difficult LSB targets to give unique results. But we do find that useful constraints can still be extracted by simulating what is expected to be observed for various hypothesized halo potentials.

The paper is organized as follows. In Section 2, we describe the simulations. The axisymmetric NFW potential is explored in Section 3. In Section 4, we describe the mock velocity fields and rotation curves produced by a nonaxisymmetric NFW potential with a constant axis ratio. In Section 5, we determine the nonaxisymmetric potentials that best describe the observed galaxy data. We discuss our results and conclusions in Section 6.

2. DESCRIPTION OF SIMULATIONS

N-body simulations show that CDM halos of all masses can be described by the NFW potential (Navarro et al. 1996, 1997) and its variants (e.g., Diemand et al. 2005; Moore et al. 1999; Navarro et al. 2004; Reed et al. 2003). These cuspy halo potentials show a steep rise in the mass density toward the center of the halo. Most theoretical estimates of the inner slope of the halo mass density profile are as steep or steeper than that of NFW, so we choose to simulate the NFW halo as the conservative case. If the NFW potential predicts a dark matter halo with a steeper density profile than is allowed by the observed galaxy data, then even more steeply rising potentials are automatically excluded. In some formulations (e.g., Navarro et al. 2004), there is no well defined inner slope, which continues to roll over to a value that asymptotes to a flatter value than NFW. However, this is a small effect at small radii. The difference between the original NFW profile and that of Navarro et al. (2004) is too small to be detected observationally.

Table 1
Simulated NFW Halo Parameters

Galaxy (1)	c (2)	V_{200} (km s^{-1}) (3)	$R_{\rm excess}$ ($''$) (4)
NGC 4395	8.6	87	59
DDO 64	9.2	62	40
UGC 4325	6.9	249	40
F583-1	8.7	83	37
F563-1	8.4	101	13
F583-4	9.1	67	22
UGC 5750	9.1	67	31
F563-V2	7.9	130	22
F568-3	8.2	110	13

Notes.
Columns (2) and (3) list the NFW halo parameters for the simulated galaxies. Listed in column (4) are the radii at which the observed DensePak rotation curves and input NFW$_{\rm constr}$ rotation curves overlap in the minimum disk case. These are the radii out to which the observed and mock rotation curves are compared.

In K06 and K08 we defined a constrained NFW halo, NFW$_{\rm constr}$. We required the halo to match the velocities at the outer radii of each galaxy by choosing a value of V_{200} which forced the NFW velocities to agree with the data points at large radii with the minimum requirement of falling within the error bars of the data. We then used the c–V_{200} relation (Navarro et al. 1997; de Blok et al. 2003) to determine the corresponding cosmologically consistent concentration. This is adjusted to the "vanilla" cosmology of Tegmark et al. (2004) by subtracting 0.011 dex in concentration (see McGaugh et al. 2003). According to ΛCDM, these are the rotation curves that our galaxies should have. The chief remaining uncertainty in the normalization of the c–V_{200} relation is the power spectrum. Rotation curve data prefer lower σ_8 (McGaugh et al. 2007).

Our goal is to compare mock DensePak velocity fields and rotation curves of NFW$_{\rm constr}$ halos with the observed DensePak velocity fields and rotation curves of the LSB galaxies in K06 and K08. We model those galaxies that have well sampled velocity fields and rotation curves that are constrained at large radii by previous long-slit and/or H I rotation curves, allowing NFW$_{\rm constr}$ halo fits to be made. Of our 17 galaxies, nine meet these criteria. The spatial resolution and DensePak coverage of these data vary. The parameters of the NFW$_{\rm constr}$ halos in the limit of minimum disk (K06; K08) for each of the nine modeled galaxies are listed in Table 1. The galaxies are listed in order of decreasing spatial resolution, from NGC 4395 ($\sim$ 20 pc/$''$) to F568-3 ($\sim$ 375 pc/$''$).

We developed a code that does a fourth-order Runge–Kutta (RK4) test particle integration of point masses moving in a two-dimensional rigid analytic NFW potential. Specifically, the potential used is

$$\Phi(R) = -\frac{GM_{200}\ln(1+\frac{R}{R_s})}{Rf(c)}, \quad (1)$$

where

$$R = \sqrt{x^2 + (y^2/q^2)}, \quad (2)$$

$$R_s = \frac{R_{200}}{c}, \quad (3)$$

and

$$f(c) = \ln(1+c) - \frac{c}{1+c}. \quad (4)$$

In these equations, M_{200} is the enclosed halo mass at radius R_{200}, q is the axis ratio ($q = y/x$), and c is the concentration of the halo ($c = R_{200}/R_s$). The halo parameters are set to those of the NFW$_{\rm constr}$ halo determined for each galaxy in K06 and K08, and are listed in Table 1. Each simulated galaxy is an infinitely thin exponential disk of 10,000 test particles. For the nearby galaxies UGC 4325 and DDO 64, the number of test particles was increased to 100,000 to ensure sufficient sampling of particles to recreate the higher resolution data. The two-dimensional disk is in the plane of the potential. To wash out any numerical pattern noise of the initial conditions, we integrate for 50 half-mass rotation periods having 500 timesteps each. Each simulated galaxy is given the disk scale length, spatial resolution, and inclination of the real galaxy.

Each simulated galaxy is then "observed" by DensePak. DensePak is an integral field spectrograph on the 3.5 m WIYN telescope at the Kitt Peak National Observatory (KPNO). It is a $43'' \times 28''$ fixed array of $3''$ fibers with $3''.84$ separations. We model the 85 working fibers, as well as the five missing or broken fibers, in the main bundle. For the galaxies observed in K06 and K08, the fiber bundle orientation on the sky and the total number of pointings per galaxy were tailored to each galaxy so that the critical central regions were covered by the DensePak fibers. We aim for obtaining roughly equivalent coverage of the simulated galaxies by using similar numbers and alignments of DensePak pointings on the simulations. Prior to extracting a rotation curve, these mock DensePak velocity fields are given the velocity dispersion observed in the real DensePak galaxy velocity fields. We have defined the velocity dispersion of the DensePak data to be the fiber-to-fiber velocity variation; to recreate this in the mock data, we randomly add the desired dispersion to the fibers in the mock velocity field. Rotation curves were then derived from the mock DensePak observations by using the NEMO (Teuben 1995) program ROTCUR (Begeman 1989). ROTCUR treats the observed velocity field as an ensemble of tilted rings and fits for the center, systemic velocity, inclination, position angle, and rotation velocity in each ring. The reader is referred to K06 and K08 for a more extensive explanation of ROTCUR and its application to the DensePak velocity fields.

3. AXISYMMETRIC NFW HALOS

The most obvious and simple starting point is to assume an axisymmetric halo potential. The axis ratio q is equal to 1 and the test particles move on circular orbits. With this straightforward potential, we can test whether or not DensePak observations are sufficient to detect the signature of NFW halos in the velocity fields and/or whether the data analysis procedure with ROTCUR also suffices to recover NFW rotation curves.

In Figure 1, we model the NFW$_{\rm constr}$ halo of UGC 4325 and "observe" the simulation with five pointings of the DensePak array. The pointings are arranged to match the spatial coverage of the real galaxy as much as possible. Observed and residual velocity fields for both UGC 4325 and the simulation are shown. The simulated galaxy has the same fiber-to-fiber velocity dispersion as the real galaxy: $\sigma = 9.0$ km s^{-1}. UGC 4325 is one of the most nearby ($D \approx 10$ Mpc) and well resolved galaxies in our sample. Diffuse Hα emission was abundant in the galaxy and was detected in almost all of the DensePak fibers.

Figure 1 demonstrates two important points. First, as evidenced by the very small residuals of the mock DensePak velocity field, the DensePak instrument *is* able to successfully detect an NFW velocity field. The residuals are generally $\lesssim 5$ km s^{-1} across the entire observed area. This means that observed DensePak velocity fields are not inconsistent with NFW halos because of an inadequacy of the experimental design or analysis. Second, the observed DensePak velocity field of UGC 4325 is not consistent with the axisymmetric NFW$_{\rm constr}$ halo; most of the residuals are ~ 10 km s^{-1}, and there is a significant region of ~ 15 km s^{-1} residuals near the center. For UGC 4325, and the other LSB galaxies in our sample, 15 km s^{-1} residuals are nontrivial. The observed fiber-to-fiber velocity dispersions are $\sim$ 6–10 km s^{-1} (K06), and since mass scales as σ^2, the implied mass difference is a factor of two or more. In addition, noncircular motions caused by disk instabilities, such as spiral or bar modes, are expected to be small in LSB galaxies. The low surface mass densities of the disks provide little self-gravity to drive such modes, and their high dark matter content provides a higher degree of stabilization than in high surface brightness galaxies (Mihos et al. 1997).

At the bottom of Figure 1 are the observed and mock rotation curves derived from the velocity fields. The recovered mock rotation curve is consistent with the input rotation curve ($\chi_r^2 = 0.93$) out to $R_{\rm excess} \sim 40''$, where $R_{\rm excess}$ is defined to

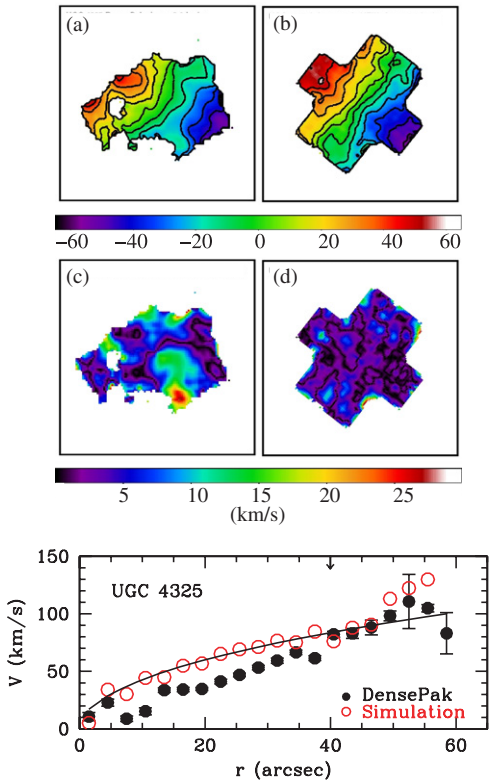

Figure 1. (a) Observed DensePak velocity field of UGC 4325. (b) Mock DensePak velocity field of the axisymmetric simulation. Both velocity fields have isovelocity contours at 10 km s^{-1} intervals. (c) Residual velocity field showing the differences between the UGC 4325 data and the velocity field of the idealized (i.e., no velocity dispersion), axisymmetric NFW$_{\rm constr}$ halo. (d) Same as (c) but for the mock DensePak velocity field. The residuals are large and obvious in (c). Bottom: observed and mock rotation curves. The solid points are the observed DensePak rotation curve of UGC 4325, the solid line is the NFW rotation curve corresponding to the input NFW potential, and the open (red) circles are the rotation curve recovered from the mock velocity field. The arrow indicates the radius out to which the rotation curves are compared. The last three points of the recovered mock rotation curve are high because of a lack of fibers at large radii.

(A color version of this figure is available in the online journal.)

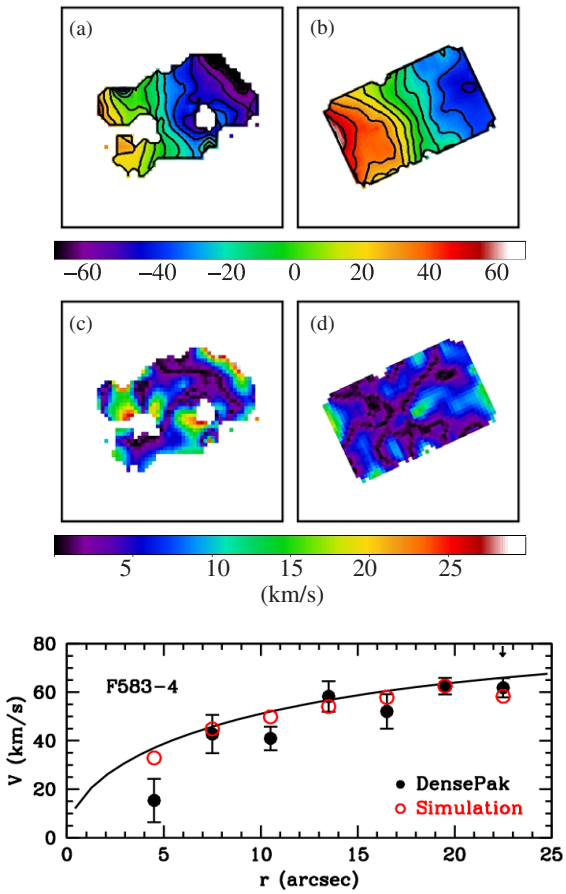

Figure 2. Same as Figure 1, but for the less well resolved galaxy F583-4.
(A color version of this figure is available in the online journal.)

be the radius at which the observed DensePak rotation curve and the input axisymmetric NFW_{constr} rotation curve begin to overlap. This shows that accurate extraction of the rotation curve of an axisymmetric NFW halo with ROTCUR is *also* possible.

In Figure 2, we show similar plots for F583-4. This galaxy has lower spatial resolution ($D \approx 49$ Mpc) than UGC 4325 and only a single pointing of DensePak coverage. The velocity fields, residuals, and rotation curves show that despite the reduced sampling and lower data quality, an axisymmetric NFW halo can still be detected if present. While the differences between the observed and mock velocity field residuals are not as pronounced as in the UGC 4325 case, the input NFW rotation curve is successfully recovered by ROTCUR ($\chi^2_r = 0.32$).

The velocity field and rotation curve data and simulations plotted in Figures 1 and 2 together show that the DensePak IFU and the tilted-ring fitting program ROTCUR are able to successfully identify an axisymmetric NFW halo in data of both high and low quality, if one is present. The K06 and K08 samples of DensePak observations are inconsistent with NFW halos suggesting that if the underlying halo potential is NFW, it must not be an axisymmetric NFW potential. This is perhaps not surprising, as CDM simulations suggest that the halo potentials are triaxial (e.g., Hayashi et al. 2007).

4. NONAXISYMMETRIC NFW HALOS WITH A FIXED AXIS RATIO

We next consider nonaxisymmetric two-dimensional NFW potentials with axis ratios $q < 1$ that are constant with radius. These two-dimensional potentials are equivalent to three-dimensional prolate dark matter halos in which the long axis of the halo coincides with the elongated axis of the disk. We simulate halos with axis ratios $q = 0.98, 0.96, 0.94, 0.92, 0.90, 0.88, 0.86$, and 0.84, similar to the range of nonaxisymmetry seen in the CDM simulations of Hayashi et al. (2007). Because axisymmetry has been broken ($q \neq 1$), the test particles no longer move on circular orbits and not all lines of sight in the plane of the disk are equivalent. This means that the observed mock DensePak velocity field and derived rotation curve are affected not only by the value of q, but also by the orientation (ϕ) of the potential's elongation with respect to the observer's line of sight (LOS; see Figure 3). The potential is elongated along the observer's LOS in the $\phi = 0°$ case, whereas in the $\phi = 90°$ case, the potential is elongated perpendicular to the observer's LOS. For $0° < \phi < 90°$, the elongation is at an intermediate viewing orientation. For each value of q, the orientation of the potential is set to $\phi = 0°, 30°, 45°, 60°$, and $90°$.

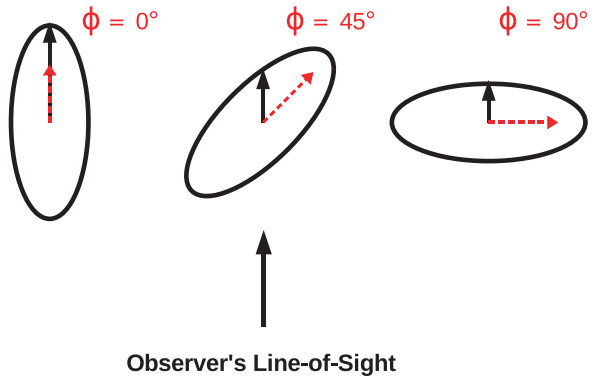

Figure 3. Orientation (ϕ) of the elongated axis of the two-dimensional nonaxisymmetric potential with respect to the observer's LOS. In the $\phi = 0°$ case, the elongated axis of the potential is along the observer's LOS, whereas in the $\phi = 90°$ case, it is perpendicular to the observer's LOS.
(A color version of this figure is available in the online journal.)

4.1. "Observed" Mock DensePak Velocity Fields

In Figures 4 and 5, we show a series of mock DensePak velocity fields for two galaxies representative of the range of data presented in K06 and K08: UGC 4325 and UGC 5750. As previously mentioned, UGC 4325 has high spatial resolution and extended DensePak coverage. As in the axisymmetric case, five pointings of the DensePak array are overlaid on these new nonaxisymmetric simulations. In contrast, UGC 5750 is a more distant galaxy ($D \approx 56$ Mpc), and both the real galaxy and the simulations have only one pointing of DensePak coverage.

These are simulations of nonaxisymmetric NFW halos that obey the cosmic c–V_{200} relation. The virial velocity V_{200} has been chosen to match each galaxy (the NFW_{constr} halos of K06 and K08). In this section, we explore the effect of introducing a nonaxisymmetric potential with equal squashing q at all radii.

In the $q = 0.98$ simulations, the potential is nearly circular. Throughout their orbits, the particles maintain a roughly constant distance from the center of the potential and as a result, have approximately constant orbital speeds. The viewing angle therefore has little effect on the observed velocity field. The $q = 0.98$, $\phi = 0° \rightarrow 90°$ mock velocity fields appear very similar, looking not only to be consistent with different realizations of the same underlying potential, but also very much like the mock velocity field of the axisymmetric potential.

The same cannot be said for the mock velocity fields of the $q = 0.88$ simulations. With orbits deviating significantly from

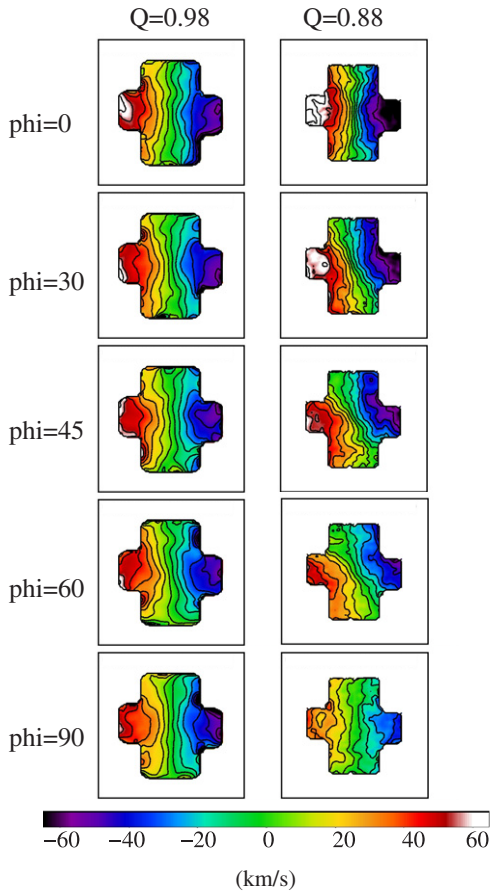

Figure 4. Mock DensePak velocity fields for the nonaxisymmetric NFW simulations of UGC 4325. UGC 4325 is a well resolved galaxy with multiple pointings of DensePak coverage. Simulations with an axis ratio $q = 0.98$ are shown in the left column and simulations with $q = 0.88$ are in the right column. The observer's viewing angle changes from $\phi = 0°$ in the top panels to $\phi = 90°$ in the bottom panels. Note that the effect of the viewing angle is much more pronounced in the $q = 0.88$ case. For easy comparison, all of the velocity fields are on the same color/velocity scale, and isovelocity contours are drawn at 10 km s^{-1} intervals.

(A color version of this figure is available in the online journal.)

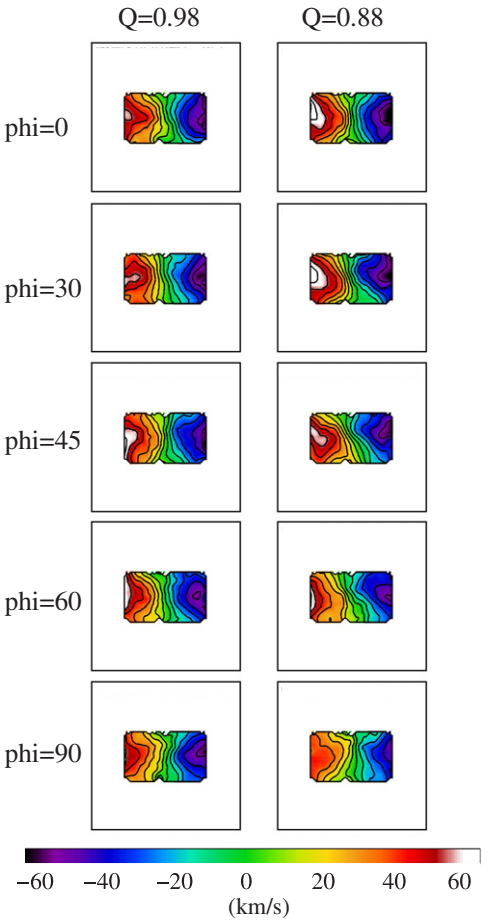

Figure 5. Same as Figure 4, but for the mock DensePak velocity fields for the nonaxisymmetric NFW simulations of UGC 5750. UGC 5750 is a more distant galaxy and has only a single pointing of DensePak coverage.

(A color version of this figure is available in the online journal.)

circular, a particle's orbital speed depends on its location, making the viewing angle quite important. In the $\phi = 0°$ orientation, the particles moving along the observer's LOS travel along the long axis of the potential and are moving at the maximum orbital speed. These particles move faster than particles on circular orbits at the same radius. The minimum–maximum velocity range observed by DensePak is larger than what is observed in the axisymmetric case, and the derived rotation curves will reach higher velocities. The opposite situation happens in the $\phi = 90°$ orientation. In this case, the particles moving along the observer's LOS travel at the minimum orbital speed, and the minimum–maximum velocity range observed by DensePak is smaller than what is observed in the axisymmetric case. The rotation curves derived from these data will therefore be suppressed. The difference between the observed velocity ranges of the $\phi = 0°$ and $\phi = 90°$ velocity fields becomes more exaggerated the more noncircular the potential becomes.

Some (q, ϕ) combinations can automatically be excluded as possible descriptions of the observed DensePak galaxy data based simply on the mock velocity fields they produce. The observed DensePak galaxy velocity fields put constraints on the allowable velocity range of the mock velocity fields, as well as the correlation between the velocity and position. Regardless of how the mock rotation curves may turn out, if the observed and mock velocity fields do not match, the corresponding simulation is not a viable solution. For example, the $(q, \phi) = (0.88, 0°)$ mock velocity field of UGC 4325 shown in Figure 4 can rule out that particular axis ratio/viewing orientation combination for that galaxy. Overall, the mock velocity field covers a much larger velocity range than the UGC 4325 data, and when the velocities at the same positions in the two velocity fields are compared, they are inconsistent over a large portion of the observed area.

Because of the rapidly rising velocities at the centers of NFW halos, the isovelocity contours of NFW velocity fields are pinched in the central regions (de Blok et al. 2003). This pinch is a distinctive signature of the cuspy NFW halo. If the velocity field is noisy or has high velocity dispersion, the pinch is more difficult to see. We can quantify the pinch by measuring velocities along slits that are offset from, and parallel to, the minor axis of the velocity field. It is in this fashion that we compare the appearance of the UGC 4325 DensePak velocity field and three mock velocity fields. In Figure 6, we have placed a $3'' \times 28''$ slit (the width of a DensePak fiber and the width of the DensePak array, respectively) $6''$ away from each side of the minor axis (about the separation of two rows of DensePak fibers) of the observed DensePak velocity field of UGC 4325 and the axisymmetric NFW mock velocity field (both shown in Figure 1), as well as the $(q, \phi) = (0.88, 0°$ and $90°)$ mock velocity fields in Figure 4. When we plot the average of the

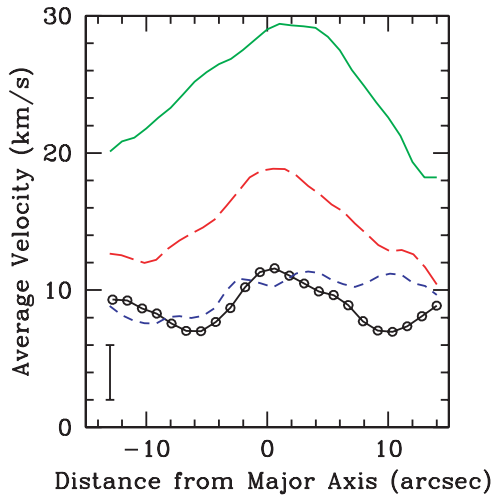

Figure 6. Comparison of three mock velocity fields to the observed UGC 4325 data using velocities measured along two slits placed parallel to, and offset from, the minor axis of the velocity fields. The solid (green) line is for the $(q, \phi) = (0.88, 0^\circ)$ mock velocity field, the long-dashed (red) line is for the axisymmetric mock velocity field, the short-dashed (blue) line is for the $(q, \phi) = (0.88, 90^\circ)$ mock velocity field, and the line + circles are the UGC 4325 data. At the same distance from the center of the velocity field, the $(q, \phi) = (0.88, 90^\circ)$ mock velocity field has velocities most similar to the observed data. A typical error bar is shown in the lower left corner.

(A color version of this figure is available in the online journal.)

measured velocities as a function of position along the slit, we can readily see that of the three mock velocity fields, it is the one produced by the $(q, \phi) = (0.88, 90^\circ)$ potential that is most like the data. At the same position in the velocity fields, the axisymmetric, and especially $(q, \phi) = (0.88, 0^\circ)$, mock observations detect velocities much higher than the galaxy data.

In Section 4.2, we derive mock rotation curves for all the mock DensePak velocity fields and examine the effect that the asymmetry of the potential has had on both the normalization and the shape of the derived rotation curves.

4.2. Derived Mock Rotation Curves

The LSB galaxies observed with DensePak in K06 and K08 surely have some level of noncircular motions, but we have assumed only circular motion when deriving the rotation curves with ROTCUR; we treat the mock observations in the same way. The test particles are, by construction, no longer on circular orbits in these nonaxisymmetric potentials, but because we did not correct for this in the real data, we do not correct for it in the mock observations. Any errors in the galaxy rotation curves which may have resulted from the assumption of circular motion will be reproduced in the rotation curves of the mock observations.

In Figure 7, we show the mock rotation curves for the nonaxisymmetric simulations of the well resolved galaxy UGC

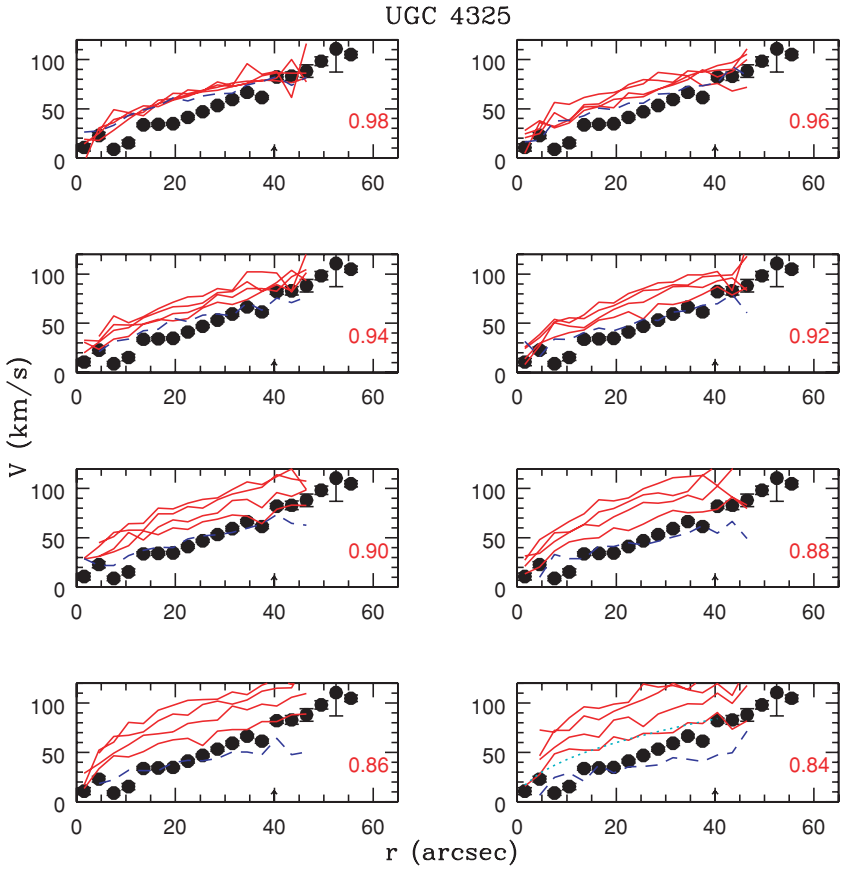

Figure 7. Mock rotation curves (lines) for the nonaxisymmetric NFW simulations of the nearby galaxy UGC 4325 (points). Each panel is for a different value of the axis ratio q (labeled in the lower right). The solid lines are for $\phi = 0^\circ$, 30°, 45°, and 60°. The dashed line is for $\phi = 90^\circ$. For all values of q, the $\phi = 90^\circ$ line has the most overlap with the data at small radii. The dotted line in the lower right panel is the input $\mathrm{NFW_{constr}}$ rotation curve. The arrows indicate the radius out to which the rotation curves are compared.

(A color version of this figure is available in the online journal.)

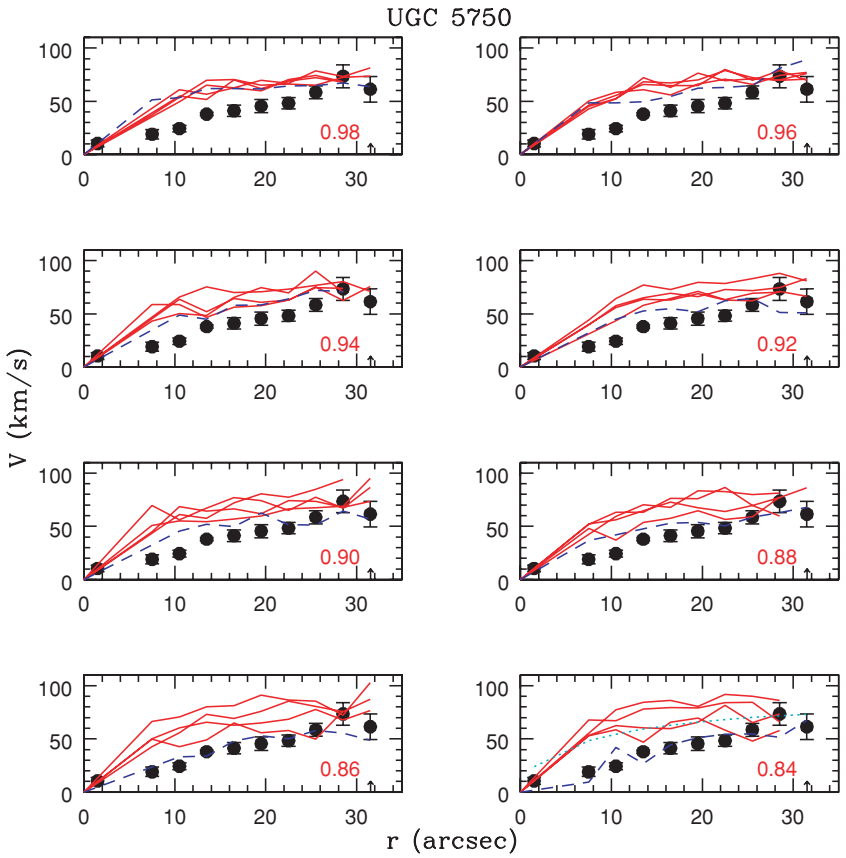

Figure 8. Same as Figure 7, but for UGC 5750.
(A color version of this figure is available in the online journal.)

4325. Each panel shows the observed rotation curve of UGC 4325 along with the $\phi = 0°$, 30°, 45°, 60°, and 90° mock rotation curves for a single value of q. Similar to the trends seen in the mock velocity fields, we find that as the axis ratio decreases and the potential becomes increasingly more elongated, the influence of the viewing angle on the inferred rotation curves becomes more striking: the mock rotation curves for the different values of ϕ spread farther out in velocity space. We can quantitatively measure and compare the shapes of these rotation curves using the ratio of the radii containing 80% and 50% of the velocity at $R_{\rm excess}$. The average values of R_{80}/R_{50} for the UGC 4325 $q = 0.98$, 0.90, and 0.86 mock rotation curves, for example, are 2.7 ± 0.7, 2.8 ± 0.8, and 3.1 ± 0.7, respectively. *This indicates that the overall shapes of the mock rotation curves do not change significantly as q or ϕ change; it is the normalization of V(r), including V_{max}, that shifts up or down.* This is an important point to recognize, as it means that simply adopting a different (lower) value of V_{200} for the underlying NFW halo (which cannot be done without ignoring cosmological constraints) will not reconcile the observed and mock rotation curves; the mock NFW rotation curve will still not fit the data properly. Though none of the mock rotation curves match the shape of the entire observed rotation curve of UGC 4325, those that are most consistent with the data at small radii are the $\phi = 90°$ mock rotation curves. This is true for all of the values of q that were simulated, but it is the $\phi = 90°$ rotation curves in the $q \lesssim 0.90$ simulations that have the most overlap with the data.

As a comparison to the well resolved observations of UGC 4325, in Figure 8 we show similar plots of the mock rotation curves for UGC 5750. Despite the lower spatial resolution, we find the mock rotation curves of UGC 5750 to behave in very much the same way as the mock rotation curves of UGC 4325. *We again see that the amplitude, not the shape, of the rotation curve changes as q and ϕ change, with the magnitude of the change becoming more pronounced as the potential becomes more asymmetric.* We also find that the $\phi = 90°$ mock rotation curves are again the closest to approaching the data, though substantial overlap at small and intermediate radii does not occur until $q \lesssim 0.86$.

In Figure 9, we examine how changing the input NFW halo parameters affects the mock rotation curves, specifically exploring if q and ϕ can change the *shape* of a more slowly rising input NFW rotation curve. For both UGC 4325 and UGC 5750, we have simulated NFW halos with low values of V_{200} and the lowest corresponding concentration within the scatter of Bullock et al. (2001) (UGC 4325: $c = 5.2$, $V_{200} = 140$; UGC 5750: $c = 6.9$, $V_{200} = 60$). These new input NFW rotation curves fall between the rotation curves representing the -1σ scatter on c and V_{200} of the original NFW$_{\rm constr}$ rotation curves. In addition, these slowly rising rotation curves overlap the observed DensePak data at small radii, in contrast to the NFW$_{\rm constr}$ rotation curves that match the data at large radii. Essentially, we choose to match the inner rather than the outer velocities with halos drawn from the favorable edge of the plausible cosmological distribution.

For both galaxies, we find the new mock rotation curves to behave similarly to the mock rotation curves in Figures 7 and 8. As the axis ratio q decreases, the mock rotation curves for the different values of ϕ scatter about the input NFW rotation curve,

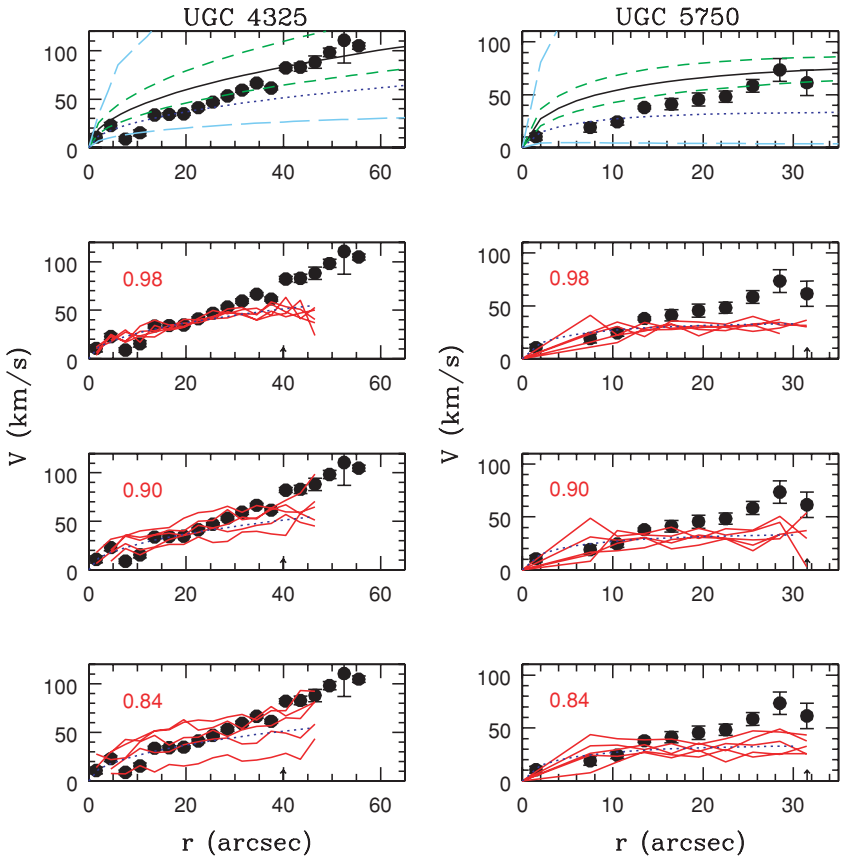

Figure 9. Top row: solid line is the NFW_{constr} rotation curve. The short dashed lines are the NFW rotation curves corresponding to the $\pm 1\sigma$ scatter (Bullock et al. 2001) expected in the concentration in ΛCDM, and the long dashed lines correspond to the $\pm 1\sigma$ scatter on V_{200}. The halo of this galaxy could plausibly be drawn from anywhere in this range. For example, the dotted line is the NFW rotation curve representing a low V_{200} and the lowest corresponding concentration within the scatter. This halo provides a good initial match to the inner data at the expense of falling well short of the outer data. Lower panels: mock rotation curves for the nonaxisymmetric NFW simulations of this low V_{200} halo (dotted lines). Each panel is for a different value of the axis ratio q (labeled in the upper left). The solid lines are for $\phi = 0°, 30°, 45°, 60°$, and $90°$. The arrows indicate the radius out to which the rotation curves are compared.

(A color version of this figure is available in the online journal.)

spreading farther out in velocity space. Even though these new mock rotation curves overlap some of the observed DensePak data at small radii, none are formally acceptable fits ($\chi_r^2 \gg 1$). More importantly, the shapes of the mock rotation curves do not significantly change as q and ϕ change: the average values of R_{80}/R_{50} for the UGC 4325 $q = 0.98$, 0.90, and 0.84 mock rotation curves are 2.3 ± 0.3, 2.8 ± 0.4, and 3.1 ± 1.2. The mock UGC 5750 rotation curves are essentially flat between $\sim 10''$ and $\sim 30''$, preventing useful measurements of R_{80}/R_{50}. From Figure 9, we can see that regardless of the input NFW halo parameters, q and ϕ change only the normalization, not the radial behavior, of the mock rotation curves.

It is also worth stressing that, given the behavior of the mock rotation curves in Figures 7 and 8, as well as Figure 9, observers should see rotation curves with a range of normalizations: there should be rotation curves both above and below the nominal rotation curve expected from the c–V_{200} relation (compare the mock rotation curves to the dotted lines in Figure 9 and the lower right panels of Figures 7 and 8). But this is, in fact, not what is observed in long-slit data (McGaugh et al. 2001; de Blok & Bosma 2002). LSB and NFW rotation curves nearly always differ in the sense that the observed rotation curve velocities at small radii must increase so that the data match the models or, equivalently, the NFW rotation curve velocities must decrease so the models match the data. LSB rotation curves which are higher than NFW rotation curves are seldom found, if ever.

There is a trade-off between q and ϕ such that different combinations of the two parameters can produce similar mock rotation curves. In Section 5, we explore what combination of (q, ϕ) minimizes the differences between the NFW halo and the DensePak galaxy observations. We simulate the NFW_{constr} halos rather than low V_{200} halos like those in Figure 9 because the constrained halos were required to match the velocities at the outer radii of each galaxy, a reasonable constraint since dark matter must explain the high velocities at large radii where the contribution of the baryons has fallen off. Parameter space is too large to explore all possible initial halos. However, given that plausible combinations of NFW c and V_{200} parameters give rather degenerate rotation curves, and that q and ϕ affect only the normalization, not the shape of $V(R)$, our choice should lead to fairly general results.

5. MINIMIZING THE CUSP MASS EXCESS WITH q AND ϕ

In K08, we showed that there is a substantial cusp mass excess near the centers of the galaxies when the NFW_{constr} halo is used to describe the dark matter halo. Evaluating the difference between the NFW_{constr} rotation curve and the observed galaxy rotation curve in terms of mass rather than

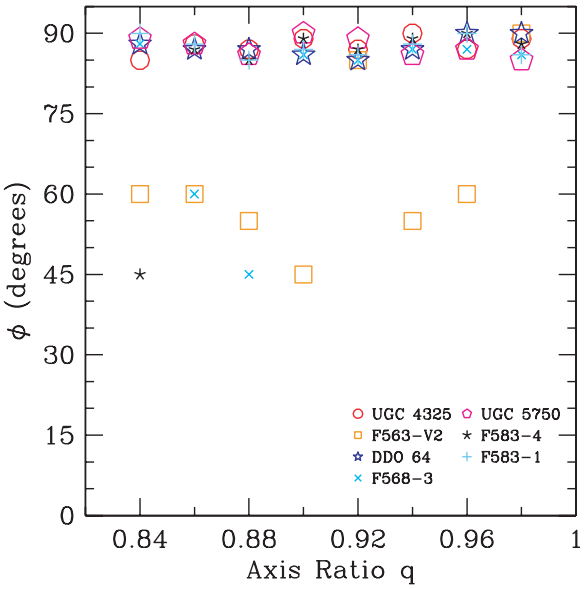

Figure 10. Viewing angle ϕ that minimizes the differences between the mock and observed galaxy rotation curves out to $R_{\rm excess}$ for each value of q for each galaxy. Nearly all of the galaxies fall on top of each other in the $\phi = 85°$–$90°$ range for all values of q. The optimal viewing angle for F563-V2 (open squares) is $\phi \sim 55°$; there is a stellar bar at this position angle. The results for F563-1 and NGC 4395 are not shown because ϕ is unconstrained due to the radial extent of the data. Nevertheless, the fact that we detect the bar in F563-V2 is an encouraging confirmation of the method.

(A color version of this figure is available in the online journal.)

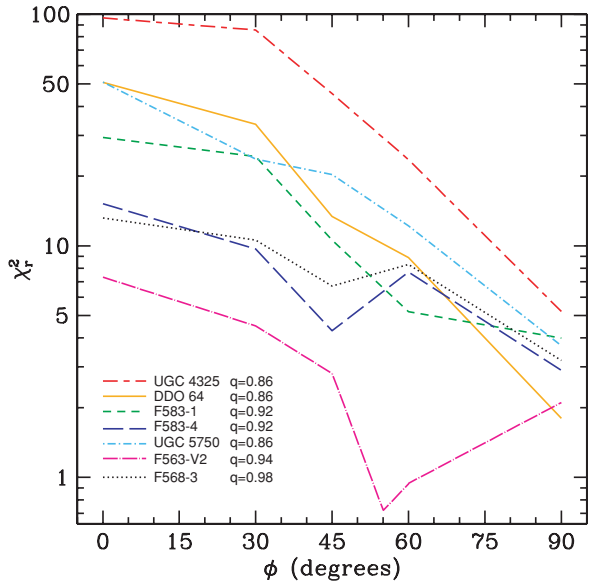

Figure 11. Value of χ_r^2 as a function of ϕ for the best-fitting q for each galaxy. Although the $\phi \rightarrow 90°$ mock rotation curves are not formally good fits to the observed data, they are the minimum in χ^2-space. The exception is F563-V2, for which $\chi_r^2 \approx 1$ for the optimal viewing angle of $\phi \approx 55°$.

(A color version of this figure is available in the online journal.)

velocity, we determined that interior to the radius where the two rotation curves begin to overlap ($R_{\rm excess}$), NFW halos are at least twice as massive as the galaxy data will allow. In this section, we are interested in determining for each DensePak galaxy what combination of (q, ϕ) minimizes the differences between the observed and mock rotation curves out to $R_{\rm excess}$ where, in the limit of zero stellar mass, the cusp mass excess is ~ 0 (see Table 1). In this fashion, one can imagine a toy model in which the halo of a particular galaxy is squashed to the best-fit (q, ϕ) within $R_{\rm excess}$ while outside of $R_{\rm excess}$ we have a more nearly spherical, cosmologically consistent NFW$_{\rm constr}$ halo.

Figures 7 and 8 showed that regardless of the axis ratio, the mock $\phi = 90°$ rotation curves came closest to the observed rotation curves of UGC 4325 and UGC 5750. To confirm that the differences between the rotation curves derived from the simulations and from the observed galaxy data are really minimized at $\phi \approx 90°$ and not somewhere between $\phi = 60°$ and 90°, we ran additional simulations at $\phi = 75°$, 85°, 86°, 87°, 88°, and 89°. We then determined for each combination of q and ϕ how well, as measured by χ_r^2, the mock and observed rotation curves matched out to $R_{\rm excess}$.

In Figure 10, we plot the best ϕ for each value of q for each galaxy. For nearly all of the nine simulated galaxies, the mock rotation curves are most consistent with the DensePak galaxy rotation curves when ϕ is between 85° and 90° for all values of q. $\phi \rightarrow 90°$ means that the elongated axis of the NFW potential points perpendicular to our LOS. This required ϕ is completely inconsistent with a random distribution of halo orientations on the sky.

There is one galaxy in our sample, F563-V2, which has a preferred value of ϕ *other* than 90°. This galaxy has a bar in it (Pildis et al. 1997). We ran additional simulations for F563-V2 and found that $\phi \approx 55°$ is the optimal viewing angle for matching the mock rotation curves to the observed rotation curves. This position angle matches that of the bar. It would therefore seem that we have detected the expected noncircular motion associated with the bar rather than the squashing of the halo (see also Spekkens & Sellwood 2007).

This result for F563-V2 confirms that we *are* able to detect the presence and orientation of an asymmetry in a velocity field. If the other DensePak galaxies contain bars or are embedded in nonspherical NFW halos, we would be able to detect the asymmetry. All the other DensePak galaxies have $\phi \approx 90°$ demonstrating that either the data are inconsistent with nonaxisymmetric NFW halos or that we must accept the unlikely coincidence that all of these galaxies are oriented such that the elongated axis of the potential is perpendicular to our LOS. It is not surprising that the effect goes in this sense as the rotation curves of LSB galaxies are persistently measured to be shallower than expected for NFW halos.

There are two galaxies whose results are not shown in Figure 10: F563-1 and NGC 4395. The value of ϕ is unconstrained for both of these galaxies due to the radial extent of the data. For F563-1, there are only a few data points to compare between the observed and mock rotation curves. NGC 4395 is a very nearby galaxy ($D \approx 3.5$ Mpc), and although there are many data points to compare in the rotation curves, the data probe a radius of less than ~ 800 pc.

As discussed in Section 4.2, q and ϕ can be used to change the amplitude of the NFW rotation curve. They do not, however, alter the overall shape of that rotation curve. This is reflected by high χ_r^2 values for the comparisons of the mock and observed rotation curves. Although the χ_r^2 values are typically greater than 1, the sharp decline in χ_r^2 as $\phi \rightarrow 90°$ indicates that $\phi \sim 90°$ is truly the minimum (see Figure 11), even though the mock rotation curves are not formally acceptable fits to the observed data. In Figure 12, we plot the "best-fitting" $\phi \rightarrow 90°$ rotation curves ($\phi \rightarrow 55°$ for F563-V2) over the observed galaxy data for each galaxy. The two galaxies with the highest spatial resolution, DDO 64 and UGC 4325, are clear examples of how the mock

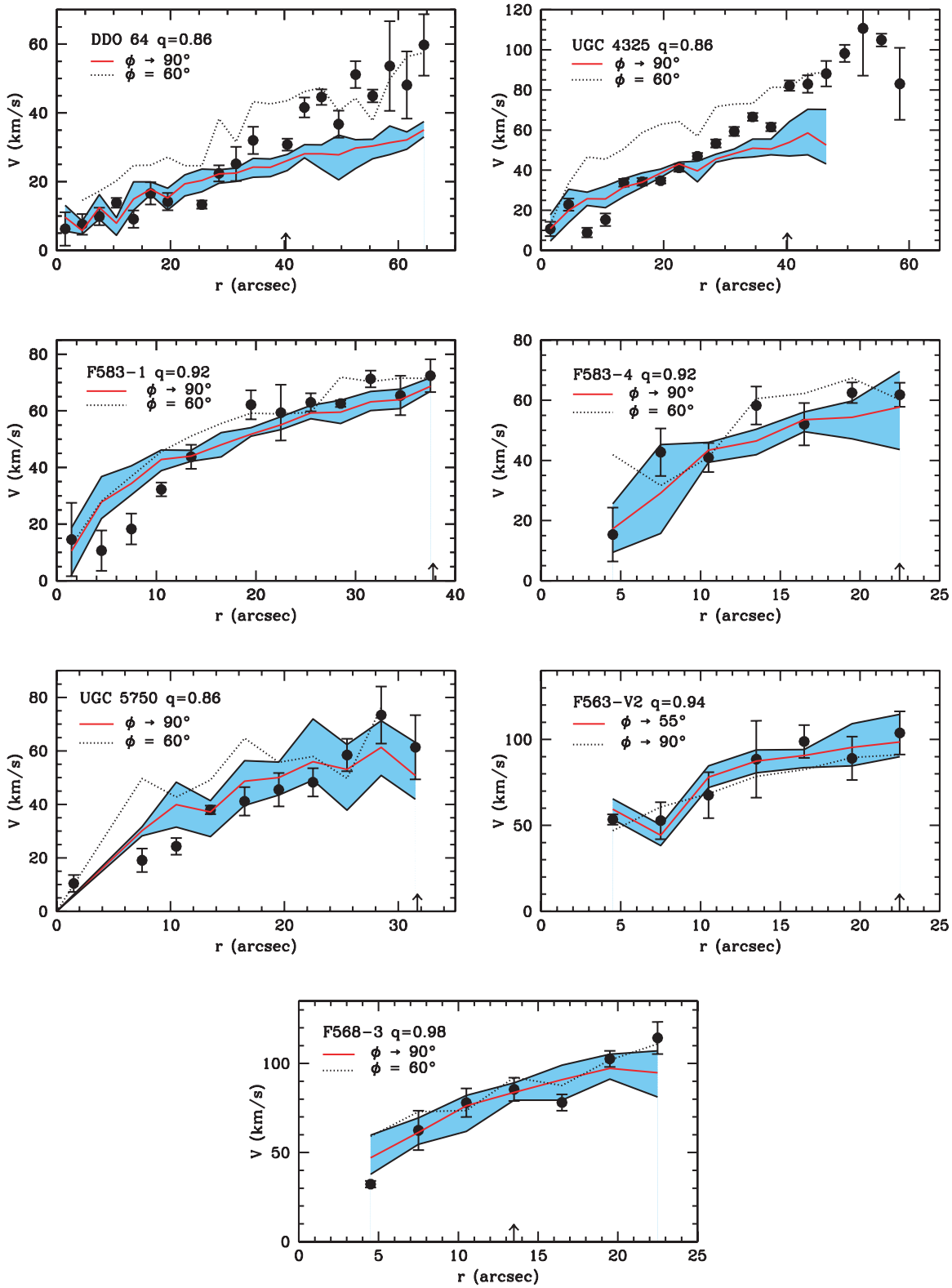

Figure 12. "Best-fitting" $\phi \rightarrow 90^\circ$ rotation curves ($\phi \rightarrow 55^\circ$ for F563-V2) for each galaxy. The solid (red) line is the average of the $\phi = 85^\circ \rightarrow 90^\circ$ ($\phi = 45^\circ \rightarrow 60^\circ$) rotation curves and the shaded (blue) band outlines the spread in those rotation curves. For comparison, the dotted line is one realization of the $\phi = 60^\circ$ ($\phi = 90^\circ$) rotation curve. The arrow indicates $R_{\rm excess}$. From top to bottom, the galaxies are ordered by increasing distance. The simulations of UGC 4325 do not extend to the outermost observed rotation curve point. The inner $7''$ of the mock rotation curves of UGC 5750 are poorly sampled, as in the real data. The results for F563-1 and NGC 4395 are not shown because ϕ is unconstrained.

(A color version of this figure is available in the online journal.)

rotation curve has shifted down in velocity such that the inner half of the mock rotation curve is roughly consistent with the observed data, but the outer half of the mock rotation curve falls below the observed data.

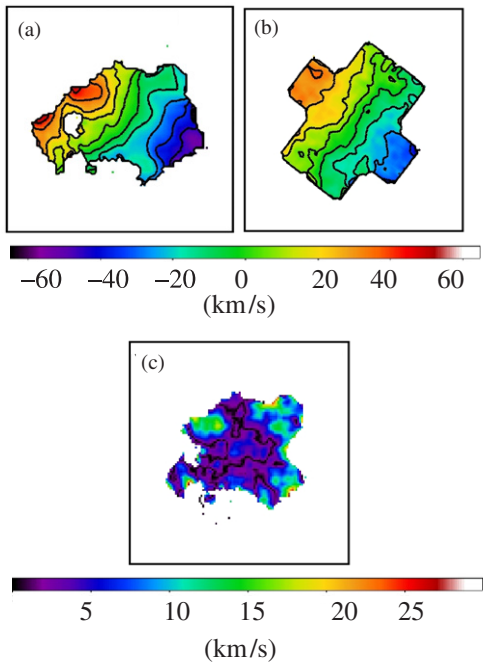

Figure 13. (a) Observed DensePak velocity field of UGC 4325. (b) The "best-fitting" nonaxisymmetric $\phi = 90°$ mock NFW velocity field of UGC 4325. (c) Residual velocity field showing the difference between the observed and mock velocity fields. The velocity fields are similar in the central regions, but become more mismatched at large radii.

(A color version of this figure is available in the online journal.)

Despite not being able to fully match the observed galaxy rotation curves within $R_{\rm excess}$, the important trend in Figures 10 and 11, and reinforced by Figures 4–6, is that ϕ is being driven toward 90° if one wants to match the observed data at small radii where the cusp/core problem is most severe. This means that the elongated axis of the NFW potentials for every DensePak galaxy (with the exception of the barred galaxy F563-V2) must point perpendicular to our LOS. This required ϕ is completely inconsistent with a random distribution of halo orientations on the sky. A nonaxisymmetric potential with a fixed axis ratio may be able to bring *parts* of the NFW rotation curve into agreement with the observed data for individual galaxies, but in general, very peculiar, observer-dependent conditions must occur.

It is worth mentioning here that the mismatches between the "best-fitting" mock rotation curves and the data, as seen in Figure 12 for example, are a result of real differences in the velocity fields; information is not being lost or suppressed as ROTCUR collapses all the data contained in the two-dimensional velocity fields into a one-dimensional representation of the rotation. As was shown in Figures 4 and 5, the lowest velocity portions of a particle's orbit are being preferentially observed in the $\phi = 90°$ viewing orientation, ensuring that the observed range of velocities detected in the mock velocity fields is both small and slowly varying. But like the rotation curves show, only some parts and not all of the observed and mock data can be made to match. In Figure 13, the observed UGC 4325 DensePak velocity field, the "best-fitting" $\phi = 90°$ velocity field, and the residual velocity field showing the differences between the two are shown as an example. While the residuals are relatively small in the central regions of the velocity field, there are multiple areas at larger radii where the residuals are in the range of $\sim$ 10–15 km s^{-1}, or more. As was discussed in Section 3, in galaxies where the fiber-to-fiber velocity dispersions are measured to be $\sim$ 6–10 km s^{-1}, 15 km s^{-1} residuals imply a significant mismatch.

6. DISCUSSION AND CONCLUSIONS

In this paper, we have simulated the two-dimensional NFW halo and tested several modifications to the potential in an attempt to simultaneously reconcile both the NFW velocity field and rotation curve with observed DensePak galaxy data. We have found that it is difficult to make the cuspy NFW halo appear consistent with core-like data without violating the predicted range of NFW parameters expected in the ΛCDM cosmological model.

Beginning with simulations of an axisymmetric NFW potential, we found that both the DensePak IFU instrument and the rotation curve fitting program ROTCUR are able to successfully identify the NFW potential. Observed galaxy data are inconsistent with the velocity fields and rotation curves corresponding to axisymmetric NFW potentials. The simulated observations show that our data would detect the NFW cusp if it were present.

We also tried a nonaxisymmetric potential with a fixed axis ratio. We found that if the parameters of the NFW halo (determined from the c–V_{200} relation) are held constant and only the axis ratio and viewing orientation are varied, parts of the mock velocity fields and mock rotation curves, but not their entire area or length, could be made to roughly match the observed galaxy data. The axis ratio and viewing orientation work to *change only the normalization, not the radial behavior*, of the mock data. The shape of the predicted NFW rotation curve remains distinct from the observations. This remains true even if a more slowly rising NFW rotation curve is simulated.

Only when the elongated axis of the mock galaxies is oriented perpendicular to the observer's LOS ($\phi \sim 90°$) are the critical velocities at small radii in both the velocity fields and rotation curves consistent with observations. Having all halos elongated perpendicular to our LOS is clearly not reasonable. This constraint on ϕ can be relaxed if we start with an NFW halo having a lower V_{200} (see Figure 9), *but changing the halo parameters requires that we disregard cosmological constraints*. Numerical simulations have shown that scatter in the c–V_{200} relation exists ($\Delta(\log c) = 0.18$; Bullock et al. 2001), but this is not enough to "fix" the mock NFW data, as the values of the halo parameters would have to be outside the range of the allowable dispersion. Furthermore, even though lowering V_{200} allows for more scatter in ϕ, the problem with the shape of the mock NFW rotation curve remains unresolved.

In order to reconcile both the entire area of the NFW mock velocity fields and the entire length of their derived rotation curves with galaxy data, we need an asymmetry that preferentially suppresses velocities at small radii. The asymmetric NFW potentials with fixed axis ratios that we have tested in this paper have altered the velocities at *all* radii, either suppressing all the measured velocities (the $\phi = 90°$ case) or boosting all of them (the $\phi \rightarrow 0°$ cases). One possible way to address this problem may be to invoke a nonaxisymmetry that varies with radius (Hayashi et al. 2007). Hayashi et al. (2007) have suggested that galaxy-sized CDM halos are triaxial with radially varying axis ratios. They found the halo potential to be highly elongated near the center ($b/a \rightarrow 0.78$ and $c/a \rightarrow 0.72$) and increasingly more spherical at large radii. This is the general behavior that the results of our two-dimensional simulations suggest is required.

It remains to be seen though if such an asymmetry is a viable solution to the problem. The simulations will always be constrained by the fact that LSB galaxy velocity fields and rotation curves are slowly rising. This will lead to the problem of a preferential viewing angle that we have already encountered. Any

potential that deviates significantly from axisymmetry at the center will have to be viewed at an angle which lowers, not increases, the observed velocities; the inner ellipsoid will need to be perpendicular to the LOS. However, if one insists that a radially varying asymmetry *is* the correct solution and that the viewing orientation is randomly distributed, both slowly and rapidly rising LSB galaxy rotation curves should be observed. LSB galaxy rotation curves that are steeper than NFW rotation curves are generally not found. Of the 50+ long-slit rotation curves in the literature (e.g., Zackrisson et al. 2006; Spekkens et al. 2005; de Blok & Bosma 2002; McGaugh et al. 2001), it is very common to see slowly rising rotation curves, but exceedingly rare to see rotation curves that are in excess of the expectation for NFW halos that obey the ΛCDM c–V_{200} relation.

The analysis of an NFW potential with a variable axis ratio is sufficiently complex that if one is to do it right, it should be done in three dimensions with interacting particles. If having a highly elongated potential is key to "fixing" the NFW velocity field and rotation curve, then adiabatic contraction should also be considered, as it will round out the inner halo potential (Dubinski 1994; Bailin et al. 2007). Adiabatic contraction also has the effect of increasing the dark matter density of the halo over its initial value and serves to worsen the concentration problem (e.g., Gnedin et al. 2004; Sellwood & McGaugh 2005). We therefore defer the analysis of a radially varying axis ratio to a forthcoming paper in which the complexity of the simulations is increased by moving to three dimensions and including gas physics.

We thank the referee for a thorough, detailed, and constructive report. The work of R.K.D. and S.S.M. was supported by NSF grant AST0505956. R.K.D. is also supported by an NSF Astronomy & Astrophysics Postdoctoral Fellowship under award AST0702496. This paper was part of R.K.D.'s Ph.D. dissertation at the University of Maryland. J.C.M. is supported by NSF grants AST0607526 and AST0707793.

Note Added in Proof. After completion of this paper, a preprint (Navarro et al. 2008, arxiv:0810.1522) appeared in which it was suggested that the Einasto profile fits simulated halos better than the NFW formula. From an observational perspective, the difference between these two is indistinguishable on the scales we consider here, so our conclusions remain unchanged.

REFERENCES

Bailin, J., Simon, J. D., Bolatto, A. D., Gibson, B. K., & Power, C. 2007, ApJ, 667, 191
Begeman, K. 1989, A&A, 223, 47
Bolatto, A. D., Simon, J. D., Leroy, A., & Blitz, L. 2002, ApJ, 565, 238
Borriello, A., & Salucci, P. 2001, MNRAS, 323, 285
Bosma, A. 1981, AJ, 86, 1825
Bullock, J. S., Kolatt, T. S., Sigad, Y., Somerville, R. S., Kravtsov, A. V., Klypin, A. A., Primack, J. R., & Dekel, A. 2001, MNRAS, 321, 559
Chemin, L., et al. 2004, IAUS, 220, 333
Côté, S., Carignan, C., & Freeman, K.C. 2000, AJ, 120, 3027
de Blok, W. J. G., & Bosma, A. 2002, A&A, 385, 816
de Blok, W. J. G., Bosma, A., & McGaugh, S. S. 2003, MNRAS, 340, 657
de Blok, W. J. G., & McGaugh, S. S. 1996, ApJ, 469, L89
de Blok, W. J. G., & McGaugh, S. S. 1997, MNRAS, 290, 533
de Blok, W. J. G., McGaugh, S. S., & Rubin, V. C. 2001, AJ, 122, 2396
de Blok, W. J. G., McGaugh, S. S., & van der Hulst, J. M. 1996, MNRAS, 283, 18
Diemand, J., Zemp, M., Moore, B., Stadel, J., & Carollo, M. 2005, MNRAS, 364, 665
Dubinski, J. 1994, ApJ, 431, 617
Flores, R. A., & Primack, J. R. 1994, ApJ, 427, L1
Fuchs, B. 2003, Ap&SS, 284, 719
Gentile, G., Burkert, A., Salucci, P., Klein, U., & Walter, F. 2005, ApJ, 634, L145
Gentile, G., Salucci, P., Klein, U., & Granato, G. L. 2007, MNRAS, 375, 199
Gnedin, O. Y., Kravtsov, A. V., Klypin, A. A., & Nagai, D. 2004, ApJ, 616, 16
Hayashi, E., Navarro, J. F., & Springel, V. 2007, MNRAS, 377, 50
Jing, Y. 2000, ApJ, 535, 30
Kuzio de Naray, R., McGaugh, S. S., de Blok, W. J. G., & Bosma, A. 2006, ApJS, 165, 461, K06
Kuzio de Naray, R., McGaugh, S. S., & de Blok, W. J. G. 2008, ApJ, 676, 920, K08
Marchesini, D., D'Onghia, E., Chincarini, G., Firmani, C., Conconi, P., Molinari, E., & Zacchei, A. 2002, ApJ, 575, 801
McGaugh, S. S., Barker, M. K., & de Blok, W. J. G. 2003, ApJ, 584, 566
McGaugh, S. S., de Blok, W. J. G., Schombert, J. S., Kuzio de Naray, R., & Kim, J. H. 2007, ApJ, 659, 149
McGaugh, S. S., Rubin, V. C., & de Blok, W. J. G. 2001, AJ, 122, 2381
Mihos, J. C., McGaugh, S. S., & de Blok, W. J. G. 1997, ApJ, 477, L79
Moore, B., Quinn, T., Governato, F., Stadel, J., & Lake, G. 1999, MNRAS, 310, 1147
Navarro, J. F., Frenk, C. S., & White, S. D. M. 1996, ApJ, 462, 563
Navarro, J. F., Frenk, C. S., & White, S. D. M. 1997, ApJ, 490, 493
Navarro, J. F., et al. 2004, MNRAS, 349, 1039
Pildis, R. A., Schombert, J. M., & Eder, J. A. 1997, ApJ, 481, 157
Reed, D., Gardner, J., Quinn, T., Stadel, J., Fardal, M., Lake, G., & Governato, F. 2003, MNRAS, 346, 565
Rubin, V. C., Thonnard, N., & Ford, W. K., Jr. 1980, ApJ, 238, 471
Sellwood, J. A., & McGaugh, S. S. 2005, ApJ, 634, 70
Schoenmakers, R. H. M., Franx, M., & de Zeeuw, P. T. 1997, MNRAS, 292, 349
Simon, J. D., Bolatto, A. D., Leroy, A., Blitz, L., & Gates, E. 2005, ApJ, 621, 757
Spekkens, K., Giovanelli, R., & Haynes, M. P. 2005, AJ, 129, 2119
Spekkens, K., & Sellwood, J. A. 2007, ApJ, 664, 204
Swaters, R. A., Madore, B. F., van den Bosch, F. C., & Balcells, M. 2003a, ApJ, 583, 732
Swaters, R. A., Verheijen, M. A. W., Bershady, M. A., & Andersen, D. R. 2003b, ApJ, 587, L19
Tegmark, M., et al. 2004, Phys. Rev., D69, 103501
Teuben, P. J. 1995, in ASP Conf. Ser. 77, Astronomical Data Analysis Software and Systems IV, ed. R. Shaw, H. E. Payne, & J. J. E. Hayes (San Francisco, CA: ASP), 398
Wechsler, R. H., Bullock, J. S., Primack, J. R., Kravtsov, A. V., & Dekel, A. 2002, ApJ, 568, 52
Wong, T., Blitz, L., & Bosma, A. 2004, ApJ, 605, 183
Zackrisson, E., Bergvall, N., Marquart, T., & Östlin, G. 2006, A&A, 452, 857
Zentner, A. R., & Bullock, J. S. 2002, Phys. Rev., D66, 043003